Effect of goethite doping using elements with different preferential oxidation states for improved reversible phosphate adsorption

Belloni, C.; Korving, L.; Witkamp, G. J.; Brück, E.; Dugulan, A. I.

DOI
10.1016/j.jece.2023.110505

Publication date
2023

Document Version
Final published version

Published in
Journal of Environmental Chemical Engineering

Journal of Environmental Chemical Engineering 11 (2023) 110505

Contents lists available at ScienceDirect

Journal of Environmental Chemical Engineering

journal homepage: www.elsevier.com/locate/jece

Effect of goethite doping using elements with different preferential oxidation states for improved reversible phosphate adsorption

C. Belloni [a,b,*], L. Korving [a], G.J. Witkamp [b,c], E. Brück [b], A.I. Dugulan [b]

[a] Wetsus, European Centre of Excellence for Sustainable Water Technology, Oostergoweg 9, 8911 MA Leeuwarden, the Netherlands
[b] Fundamental Aspects Mat & Energy Group, Delft University of Technology, Mekelweg 15, 2629 JB Delft, the Netherlands
[c] Water Desalination and Reuse Center, Biological and Environmental Science and Engineering division, King Abdullah University of Science and Technology, Saudi Arabia

ARTICLE INFO

Editor: Dong-Yeun Koh

Keywords:
Phosphate recovery
Adsorption
Regeneration
Iron oxide
Goethite doping
Oxidation state

ABSTRACT

Phosphorus (P) removal from freshwater bodies to ultra-low concentrations is fundamental to prevent eutrophication, while its recovery is necessary to close the P usage cycle. Iron oxide-based adsorbents seem promising candidates, being abundant, cheap, and easy to synthesize compounds, with good affinity for P. Affinity is the key parameter when targeting ultra-low concentrations. Also, adsorbent regeneration and re-use is fundamental for the economic viability, hence the adsorbent stability is important. Goethite, (α-FeOOH), is one of the most stable iron (Fe^{3+}) (hydr)oxide species, with higher affinity, but lower adsorption capacity (per kg) compared to other species. Doping could change goethite surface properties, to boost the adsorption capacity, while preserving the high stability and affinity for P. In this work, pure goethite was compared to goethite doped (5%at.) with different elements of different preferential oxidation states: Zn^{2+}, Mn^{3+}, and Zr^{4+}. Doping was successfully achieved for all elements, albeit Zr showed a lower Fe substitution than targeted. Zn doping increased the goethite point of zero charge and adsorption capacity (per mass and per surface area), preserving the high affinity, while Mn- and Zr- doping displayed a decrease in all the parameters. These could be explained with surface protonation as a charge compensation mechanism in Zn^{2+}-for-Fe^{3+} substitution. The regeneration test showed improved P recovery for Zr- and Zn-doped goethite. All samples remained stable throughout the whole process. This work provides promising insights on doping as a strategy to manipulate iron oxides surface properties and for developing a highly performing and long-lasting goethite-based adsorbent.

1. Introduction

Freshwater bodies eutrophication is mainly caused by excess phosphorus (P) [1,2], eventually leading to algae blooms, causing several harmful environmental and socio-economic issues [3–5]. P ends up in water bodies via municipal wastewater and agricultural run-off, being a vital and irreplaceable nutrient, which is (over)used as a fertilizer. Moreover, P is a scarce and non-renewable resource extracted from phosphate rock mines present in a few countries, and its usage is mainly linear. As Europe almost completely relies on its import [6–8], the European Commission listed phosphate as a Critical Raw Material, asking for cyclic usage and better management [6,9,10]. In this perspective, P removal and recovery technologies have been developed, especially for wastewater treatment plants (WWTP). However, WWTP effluents P concentration requirements (< 1–2 mg L^{-1}) [11] are hundred times higher than the threshold of eutrophication, as algae bloom in freshwater bodies can take place at concentrations above 10–20 μg L^{-1} [2]. This is mainly due to the soluble P fraction, phosphate (henceforth also referred to as P for simplicity), which is the bioavailable form of P and the most challenging fraction to remove. For instance, P removal via chemical precipitation in WWTP faces technical and economical limitations to reach such low concentrations [12]. Therefore, a polishing step to remove P down the so-called ultra-low concentrations (< 20 μg L^{-1}) is necessary.

Abbreviations: WWTP, Waste Water Treatment Plant; P, Phosphorus/Phosphate; NPs, Nanoparticles; M, Metal; MQ, Milli-Q Water; DW, Demineralized Water; ICP, Inductively Coupled Plasma Optical Emission Spectroscopy; TEM, Transmission Electron Microscopy; SAED, Selected Area Electron Diffraction; SSA, Specific Surface Area; pzc, Point of Zero Charge; RMSPE, Root Mean Squared Percent Error; XRD, X-Ray Diffraction; MS, Mössbauer Spectroscopy; IS, Isomer Shift; QS, Quadrupole Splitting; Hf, Hyperfine Field.

* Corresponding author at: Wetsus, European Centre of Excellence for Sustainable Water Technology, Oostergoweg 9, 8911 MA Leeuwarden, the Netherlands.
E-mail addresses: c.belloni-1@tudelft.nl, carlo.belloni@outlook.com (C. Belloni).

https://doi.org/10.1016/j.jece.2023.110505
Received 10 March 2023; Received in revised form 30 June 2023; Accepted 3 July 2023
Available online 4 July 2023

Adsorption with iron oxide-based adsorbents looks promising for reaching ultra-low P concentrations, while allowing for P recovery. Iron oxides (including hydroxides and oxyhydroxides) are abundant, cheap, and easy to synthesize compounds, which display good affinity and selectivity for P. This is because the adsorption mechanism is based on chemisorption, meaning that a chemical bond is formed between the iron oxide surface and phosphate [13]. The process can be reversed via an alkaline wash, allowing to recover P and regenerate the adsorbent, that can be reused for further adsorption cycles[14]. Many studies have been performed under laboratory conditions, favouring the development of adsorbents with high specific surface area (SSA), and thereby potentially increasing adsorption capacities. An example of that is the work performed by Wang et al. [15]. In their work, it is shown how ferrihydrite, an amorphous iron oxide species with very high SSA, offers high P-capacity and has often been preferred to other crystalline species such as goethite (α-FeOOH). However, goethite displays higher affinity for P compared to ferrihydrite [15,16]. Affinity is a parameter that provides information on the extent of interaction between the adsorbent and the adsorbate and has also been interpreted as the adsorbent capacity at low adsorbate concentrations [17]. This means that affinity provides an indication on how well an adsorbent is able to adsorb P, even at the low concentrations, making it a crucial parameter when targeting ultra-low concentrations. In this perspective, goethite is an interesting candidate for developing an adsorbent for eutrophication prevention. Moreover, P adsorption studies spent little attention to P recovery and adsorbent regeneration. Kumar et al. [12], highlighted that reusing an adsorbent for 50–100 times would make the process economically viable. Therefore, goethite, being one of the most stable iron oxide species, is promising in regard to reuse than the highly unstable ferrihydrite.

Doping could help manipulating goethite surface properties, increasing adsorption capacity while preserving its affinity and stability. Doping is a key technique in the semiconductor [18–20] and catalysis fields [21–24]. It consists in introducing an elemental impurity, for instance a metal (M), either via inclusion (in interstices) or through substitution, in a host material to alter its properties. The resulting effects depend on the properties of M, such as ionic radius, electronegativity, and oxidation state, and so on [13,25]. Natural and synthetic goethite, both pure and M-substituted goethite, have been widely investigated from a crystallographic point of view, as well as for their adsorption properties [13,26–32]. Often, these studies have been focusing on a single doped goethite sample, and different syntheses procedures were adopted. Among the different M-substituted goethite, several studies have been performed on Al^{3+}-doped goethite [27, 33–43], mainly from a crystallographic point of view, with a few focusing also on P adsorption but not on P-desorption and adsorbent regeneration. Also, a few studies on Mn^{3+}- and Zn^{2+}-doped goethite [29, 44–49] crystallographic properties are present in literature, though without addressing P-adsorption. To our knowledge, no mineral study nor attempt of synthesis has yet been conducted on Zr^{4+}-substituted goethite.

In this work, the effect of M-for-Fe substitution in goethite nanoparticles with elements of different preferential oxidation state, i.e., Zn^{2+}, Mn^{3+}, and Zr^{4+}, on its properties and the regenerative P adsorption behavior has been investigated and compared in a systematic way. In particular, the effect of these dopants on the surface charge and the consequent P-adsorption/desorption performances have been evaluated, and a regeneration of the nanoparticles has been performed. The aim of this study is to provide a coherent investigation and insights on doping as a strategy to effectively manipulate goethite properties to develop an efficient, regenerable and long-lasting adsorbent for P-recovery.

2. Materials & methods

2.1. Chemicals

Potassium dihydrogen phosphate (KH_2PO_4), sodium chloride (NaCl), 1 M sodium hydroxide (NaOH), 1 M hydrochloric acid, 37 % hydrochloric acid (HCl) and manganese nitrate hexahydrate ($Mn(NO_3)_2{\cdot}6\ H_2O$) were purchased at VWR (The Netherlands). 3-(N-morpholino) propane sulfonic acid (MOPS) and iron nitrate nonahydrate ($Fe(NO_3)_3{\cdot}9\ H_2O$) were obtained from Sigma-Aldrich (The Netherlands), and zinc nitrate hexahydrate ($Zn(NO_3)_2{\cdot}6\ H_2O$) and zirconyl nitrate ($ZrO(NO_3)_2{\cdot}xH2O$) from Alfa Aesar (Germany).

2.2. Nanoparticles synthesis

The goethite NPs synthesis was adapted from Villacís-García et al. [50] and presented here in short. 200 mL of 2.5 M NaOH CO_2-free solution was added to an Fe solution of 50 g of $Fe(NO_3)_3{\cdot}9\ H_2O$ in 825 g of the CO_2-free MQ water at 1 mL min^{-1} with a peristaltic pump (Cole--Palmer, Masterflex L/S), under N_2 bubbling and 250 rpm stirring. After NaOH addition the solution was let stirring for additional 30 min. The suspension, consisting of ferrihydrite, was aged to goethite in an oven at 60 °C for 48 h, occasionally shaking it for better homogeneity. The transformation from ferrihydrite to goethite caused the suspension to turn from dark brown to ochre.

The doped nanoparticles were synthesized following the same procedure, with the only difference of having a mixture of Fe and 5%at. M/Fe solution, for which the Zn, Mn and Zr salts were weighed accordingly. The color change in this process was from dark brown to orange/purple for Zn, to black/olive green for Mn and to a different shade of ochre for Zr.

The NPs were then separated via Buchner filtration, thoroughly rinsed with MQ water, resuspended in Demineralized Water (DW), thoroughly shaking and sonicating for 10 min at 40 kHz (Bandelin, Sonorex RM16UH). The pH was adjusted to around 7 with HCl and NaOH. The NPs were let to settle while the supernatant replaced with DW and adjusted to pH 7, until its conductivity was below 0.1 μS cm^{-1}.

The synthesized samples are referred to as G for the pure goethite, and G[Zn5], G[Mn5] and G[Zr5], based on the nominal doping.

2.3. Nanoparticles characterization

The NPs were characterized with several techniques, to retrieve as many information as possible.

The pH and conductivity of the suspensions were measured with a SevenExcellence pH/Cond meter S470, Mettler-Toledo.

The NPs mass concentration of each suspension was assessed by dry weight, drying NPs suspension aliquots in the oven at 60 °C.

The M-for-Fe %at. was verified by dissolving the NPs (upon centrifugation) in HCl 37 % acid solution and analyzing the elemental composition with a Perkin Elmer Optima 5300 DV Inductively Coupled Plasma Optical Emission Spectroscopy (henceforth referred to as ICP).

The size and shape of the pure and doped NPs were retrieved with a JOEL JEM1400-plus Transmission Electron Microscopy (TEM) with a TVIPS F416 camera operating at 120 kV. Over 200 NPs per sample were analyzed with ImageJ software to estimate the NPs size distribution. The NPs crystallinity was also qualitatively investigated with Selected Area Electron Diffraction (SAED).

Qualitative crystallinity and crystallite size estimation, and precise phase identification were obtained with X-Ray Diffraction (XRD) measurements. The diffractometer was a PANalytical X'Pert pro X-Ray mounted in the Bragg-Brentano configuration with a Cu anode (0.4 mm × 12 mm line focus, 45 KV, 40 mA). X-Ray scattered intensities were measured with a real-time multi strip (RTMS) detector (X'Celerator). The sample holder was a spinner, and the angle range for data collection was $10° < 2\theta < 100°$ with a step size of 0.008° (2θ) and

measuring time of 1 h. XRD patterns were analyzed in fingerprinting mode using the PANalytical X'Pert software.

Mössbauer spectroscopy (MS) was employed to thoroughly identify the iron oxide phases of the pure and doped samples, investigating the effect of the dopants on the goethite properties. MS was also used to assess the sample stability after regeneration. Measurements were performed at three different temperatures, 300 K, 120 K (set-up thermalization with liquid N_2) and 4.2 K (liquid He temperature), as the low temperatures promote the Zeeman splitting, helping to better identify the different species. Transmission ^{57}Fe MS spectra were collected with conventional constant acceleration or sinusoidal velocity spectrometers using a ^{57}Co (Rh) source and calibrated to α-Fe. The MS spectra were analyzed with MossWinn 4.0 software [51] to obtain some fundamental parameters for the phase identification: the isomer shift (IS) [mm s^{-1}], the quadrupole splitting (QS) [mm s^{-1}], the hyperfine magnetic field (H_f) [mm s^{-1}], as well as the peaks line-width (Γ) [mm s^{-1}] and the spectral phase contribution [%].

The surface charge of the pure and doped NPs was estimated in terms of point of zero charge (pzc), i.e., the pH at which the net surface charge of the adsorbent is neutral. The pzc was estimated adapting the salt addition method from Mahmood et al. [52], and Tan et al. [53]. The whole procedure was performed in a glovebox, with all solutions being bubbled with N_2 gas to prevent pH fluctuations, and all NPs suspensions were sonicated for 10 min before use. Shortly, 50 mL centrifuge tubes with 10 mL of 5 g L^{-1} NPs suspensions were prepared (in duplicates) with different initial pH between 5 and 10 using HCl and NaOH. The samples were placed in a shaking incubator at 150 rpm and 25 °C for 5 days, to let the solution equilibrate. The initial pH, pH_{in}, were then measured, and 0.526 of 2 M NaCl solution was consequently added to the samples, obtaining a final NaCl concentration of 0.1 M. The samples were placed in the shaking incubator for at least a week for equilibration. The final pH, pH_{fin}, was then measured and recorded for each NP sample, the pH differences, $\Delta pH = pH_{fin} - pH_{in}$, were plotted against the pH_{in} values. The data were then interpolated with two approaches: a polynomial curve applied to the whole data range; a linear function applied to the data for which ΔpH approaches zero. The pzc is the pH value at which $\Delta pH = 0$, which is the value at which the plotted curve crosses the x axis (pH_{in}). The error assigned to the pzc was ± 0.15, which is an excess approximation of the root mean squared sum of the single contributions being: ± 0.10 for pH_{in}, ± 0.05 for pH_{fin}, and ± 0.02 of the pH meter (handheld PH 20, VWR, with GE 114 WD electrode).

The specific surface area (SSA) of the NPs was estimate using Micromeritics Tristar 3000 via Brunauer-Emmett-Teller analysis. Samples of 100 mg of dried NPs were degassed overnight under Ar atmosphere at 70 °C, followed by N_2 adsorption-desorption cycles for SSA estimation. The data were analyzed with the non-local density functional theory model in the built-in software.

The NPs samples for MB, XRD and SSA measurements were centrifuged, oven-dried at 40–60 °C and grinded before being placed in the respective sample holders.

2.4. Phosphate adsorption experiments

For the P adsorption experiments, a stock solution of 500 mg L^{-1} of P in DW was prepared from KH_2PO_4 salt. Different dilutions were prepared, to obtain P concentrations of 0.1, 0.5, 0.75, 1, 2.5, 5, 7.5 and 10 mg L^{-1}, each with 20 mM MOPS as a pH buffer, and pH adjusted to around 7.2 with NaOH/HCl. This pH value was chosen as it is one of the buffering points of MOPS, which lies within the usual pH range 6–8 of WWTP effluents and surface waters. The NPs suspensions of 1 g L^{-1} were prepared and sonicated for 10 min before addition. The addition consisted of 100 mL of P diluted solutions, from which 10 mL were removed for ICP analysis, and 10 mL of NPs suspensions, for the adsorption duplicates (adsorbent concentration of 0.1 g L^{-1}), or 10 mL of DW, for the blanks, were added. The samples were then placed in a shaking incubator at 25 °C and 150 rpm for 2 days, as previous tests showed this time was more than enough to reach the adsorption equilibrium. Nevertheless, a few samples were kept running for one more week and then analyzed for control, without showing any relevant difference.

2.5. Desorption/regeneration experiments

The regeneration test was performed following an adsorption experiment similar to that performed for the adsorption equilibrium experiment. In this case, after equilibrium was reached, the pH was increased in the same solution via NaOH addition. This procedure was chosen to avoid NPs separation via centrifugation, which can cause irreversible NPs agglomeration, and long sonication to redisperse them, which can structurally affect the NPs. For these reasons it was opted for a single regeneration run and not multiple adsorption-desorption cycles. Moreover, the idea of this test is to verify whether regeneration would require more effort with doped goethite in case doping would promote a stronger NPs-to-P bond or other P removal mechanism such as surface precipitation.

The adsorption experiment preceding the regeneration step was performed preparing 100 mL solutions with P concentrations of 25 mg L^{-1} and 20 mM MOPS at pH 7.2, from which 10 mL were removed for ICP analysis, replaced by 10 mL of 3 g L^{-1} NPs suspension for the adsorption duplicates, and 10 mL of DW for the blanks. The samples were placed in a shaking incubator at 25 °C and 150 rpm for 5 days. Then, 5 mL were collected for ICP analysis while 5 mL of 1 M NaOH solution was added, increasing the pH to about 12.6. The samples were shaken at 25 °C and 150 rpm for 1 day. The solution was then analyzed with ICP and the NPs with MS. The regeneration pH was deliberately at a lower value compared to the usual pH 13–14 (0.1–1 M NaOH) to enhance the desorption differences. In fact, the main goal is to investigate whether a different P uptake mechanism (e.g., surface precipitation, stronger bond, etc.) due to doping would require higher effort for desorption. Moreover, for a single run, desorbing at pH 13–14, where usually all the P is desorbed, would not highlight any difference, and would not show any relevant information on possible NPs (synthesized at pH > 12) deterioration.

2.6. Samples analysis

All the P-based solutions were analyzed with ICP, to determine the initial concentrations, C_0 [mg L^{-1}] of the blanks and the equilibrium concentrations, C_{eq} [mg L^{-1}] of the adsorption samples. The latter were always filtered with a 25 nm pore size filter (MF-Millipore Membrane Filter, 0.025 μm pore size, Merck), with the help of a six channel NE-1600 syringe pump (New Era Pump Systems, Inc.) prior ICP samples preparation. No appreciable difference in P concentrations was observed between the filtered and unfiltered blank samples, assuming filtration to have a negligible influence on the P concentrations at these ranges. The amount of P adsorbed per mass of adsorbent, q [mg g^{-1}], was calculated with:

$$q = \frac{C_0 - C_{eq}}{m_{NPs}} V \quad (1)$$

where m_{NPs} [g] is the mass of adsorbent and V [L] is the volume of the sample.

2.7. Data analysis

The adsorption isotherms were obtained by plotting q against C_{eq} (with duplicate data) and fitting them with two adsorption isotherm models, the Langmuir [54] and the Freundlich [55] isotherm models.

The Langmuir isotherm assumes a monolayer-like adsorption with homogeneous adsorption sites and without interaction between the adsorbed adsorbate molecules. Hence, this is an ideal model, and it was

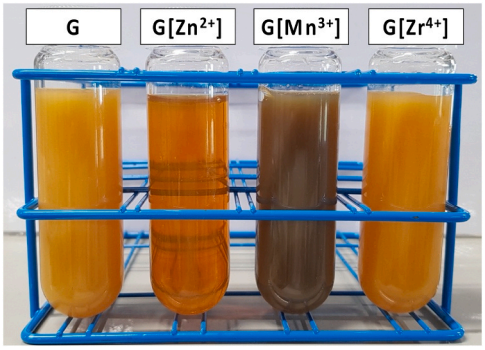

Fig. 1. The synthesized NPs suspensions (1 g L^{-1}, pH ~ 7), G, G[Zn5], G[Mn5], G[Zr5] (left to right), showing the different colors of the suspensions.

Table 1
Theoretical and experimental doping %at. from ICP analysis after NPs acid dissolution, and SSA values from BET analysis of the different synthesized NPs.

Sample	Theoretical Zn/Fe %at.	Experimental Zn/Fe %at.	SSA [m^2 g^{-1}]
G	0	0	84.7 ± 0.9
G[Zn5]	5	5.1 ± 0.3	76.0 ± 0.8
G[Mn5]	5	5.1 ± 0.3	74.2 ± 0.3
G[Zr5]	5	3.9 ± 0.2	69.4 ± 0.2

developed for gas adsorption on solid phase. The Langmuir isotherm equation is:

$$q = \frac{q_{max} K_L C_{eq}}{1 + K_L C_{eq}} \quad (2)$$

where q_{max} [mg g^{-1}], is the capacity, identified by the height of the isotherm plateau, and K_L [L mg^{-1}] is the Langmuir constant which is related to the affinity between the adsorbate and the adsorbent binding sites, identified by the steepness of the ascending part of the isotherm.

The Freundlich isotherm is an empirical model, i.e., its constants do not have a physical meaning, and it assumes adsorption to happen on a heterogeneity of sites. The Freundlich isotherm equation is:

$$q = K_F C_{eq}^{\ n} \quad (3)$$

where K_F [(mg g^{-1})(mg L^{-1})$^{-n}$] is the Freundlich constant, also called adsorption strength, which is related to the capacity of the adsorbent, and n is a dimensionless constant related to the surface sites' heterogeneity.

Given the strong limitation of the two models, the fitting parameters were evaluated carefully, as a mere mean of comparison, meaning that results were interpreted in relative terms between the different samples, rather than in absolute terms or with too much physical interpretation.

Similarly, data were also analyzed in terms of P adsorption per SSA of the NPs.

The fittings were performed using Microsoft Excel Solver,

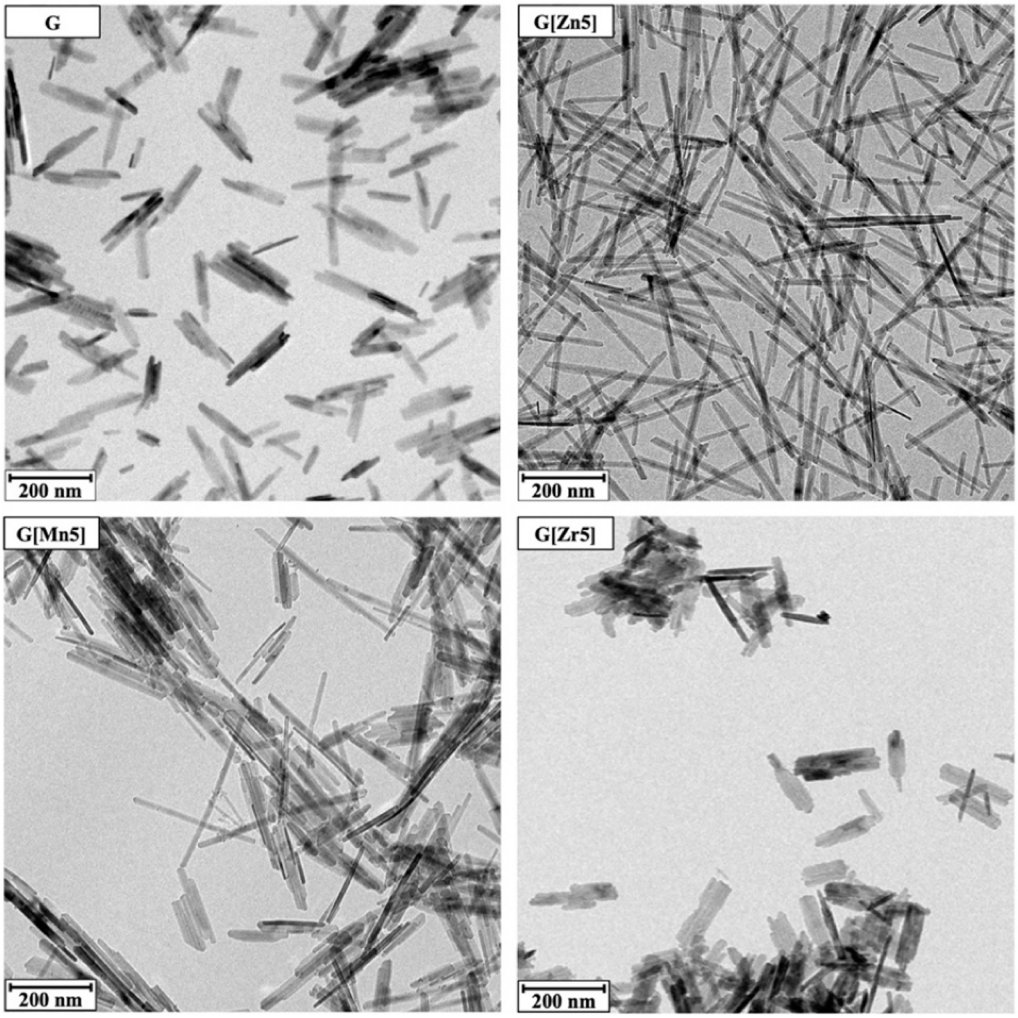

Fig. 2. TEM images of the synthesized NPs.

Table 2
Particle size estimation of the synthesized NPs from TEM images using ImageJ software.

Sample	Length [nm]			Width [nm]		
	Min	Max	Mean	Min	Max	Mean
G	11	305	102 ± 46	3	23	11 ± 3
G[Zn5]	12	330	115 ± 55	3	20	9 ± 3
G[Mn5]	13	417	133 ± 61	1	33	11 ± 5
G[Zr5]	16	196	98 ± 35	2	30	15 ± 6

minimizing the RMSPE (Root Mean Square Percentage Error), which values were reported as a measure of the goodness of the fit.

For the regeneration tests, the adsorbed P per mass and per SSA and the percentage of P desorbed have been reported in histogram plots, together with the duplicate values.

Finally, the P surface coverage percentage after adsorption and the un-desorbed P fraction after regeneration have been calculated considering a phosphate ionic radius of 238 pm [56].

3. Results and discussion

3.1. Characterization

The synthesized NPs suspensions display different colors, as visible in Fig. 1. G and G[Zr5] display different shades of ochre, G[Zn5] an orange/purple color while G[Mn5] a black/olive green color. In particular, the latter appears to be slightly attracted to strong magnets (not shown here).

3.1.1. Elemental composition and SSA measurement

The ICP elemental analysis performed on the doped samples after NPs dissolution, values are reported in Table 1, confirmed the desired 5%at. M-for-Fe substitution for Zn and Mn, while a lower Zr-for-Fe substitution ((3.9 ± 0.2) %at.) was observed. Zr^{4+} has an ionic radius of 72 pm [57], about 12 % larger than that of Fe^{3+} (64.5 pm, for high-spin Fe^{3+} in sixfold coordination, as is in goethite [57]), which falls within the ionic radius difference range for successful isomorphous substitution in goethite (< 18 %, [13]). Nevertheless a different Zr-for-Fe substitution can be expected since the ionic charge of Zr (+4) is higher than that of Fe in goethite (+3) [13]. A reason for that could be a combination of the higher charge and bigger size compared to Fe^{3+} [13], since other higher oxidation state elements like Ti^{4+}, which has a smaller radius (61 pm, [57]) than that of Fe^{3+}, was shown to successfully substitute for Fe in goethite [32].

The BET analyses show all the samples to have SSA values of the same order of magnitude, following the trend: G > G[Zn5] > G[Mn5] > G[Zr5]. SSA values are reported in Table 1.

3.1.2. TEM and SAED

The NPs morphology analysis performed with TEM, shown in Fig. 2, reveals that all the samples consist of rods, typical of goethite[13], with aspect ratio changing with doping, as expected [13]. G[Zn5] displays elongated and narrower rods, compared to G, as observed also by Krehula et al. [49]. Similarly, G[Mn5] displays elongated and narrower rods, with also the presence of filament like rods, in agreement with observations by Rout et al. [45]. Conversely, G[Zr5] NPs displayed a shortening and widening of the rods with irregular shape and a rougher surface compared to the other samples, in line with what has been reported for Sn^{4+}-doped goethite [58]. The different habit could be explained with the different mechanism of Zr substitution in goethite, causing retardation in the growth of different crystal facets compared to the other dopants. This could perhaps be related as well to the lower Zr %at. observed, suggesting that Zr is over all less prone to substitute Fe in goethite. A precise size estimation was not possible given the agglomeration of the NPs during TEM sample preparation. Thus, a more qualitative size estimation was performed with ImageJ, supporting what was previously discussed on the different aspect ratios, and the corresponding values are reported in Table 2.

SAED images, shown in Figure S.1, reveal that all the samples consist of polycrystalline NPs of goethite, as inferable from the well-defined ring patterns with intense spots.

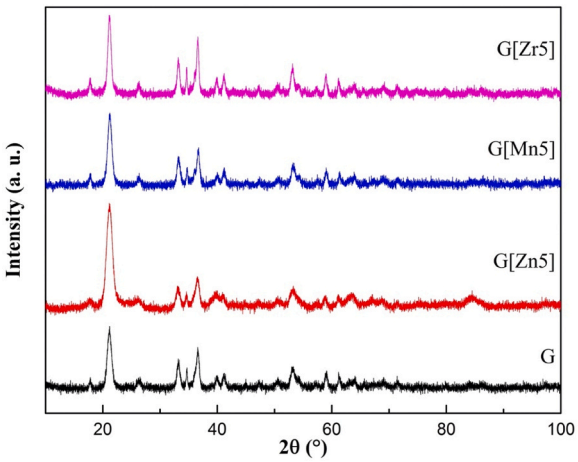

Fig. 3. XRD patterns of the synthesized NPs.

Table 3
Unit cell parameters and crystallite size estimation of the pure and doped goethite nanoparticles.

Sample	Unit cell dimensions [Å]			Crystallite size [Å]
	a	b	c	
G	9.971	3.026	4.629	120
G[Zn5]	10.096	3.019	4.613	70
G[Mn5]	9.974	3.019	4.613	105
G[Zr5]	9.898	3.025	4.633	140

3.1.3. X-ray diffraction

The analysis of the XRD patterns, shown in Fig. 3, displayed good agreement with the goethite phase for all samples, meaning that doping did not promote the formation of other iron oxide species. Differences in the peak intensity and broadening can be ascribed to different causes, such as preferential orientation, different aspect ratio, and different crystallinities of the NPs rods. These results are in agreement with SAED observations. A qualitative average crystallite size estimation for each sample has been obtained with the PANalytical X'Pert software (using peaks [110], [020], [111]). The unit cell parameters have been calculated from the XRD patterns, to highlight the distortions caused by the different dopants. These values are reported in Table 3.

3.1.4. Mössbauer spectroscopy

MS spectra are reported in Fig. 4, while Table 3 reports the fitting parameters values, together with the hyperfine parameters of bulk goethite [59]. The analyses support what was already observed with TEM-SAED and XRD, namely, the sample consist of goethite-like phases. The 300 K spectra of all samples provided IS and QS values typical of high-spin Fe^{3+} in octahedral coordination. The peaks asymmetrical broadening at 300 K is typical of the goethite phase with a distribution in particle sizes, hence a magnetic distribution fit was applied. The observed H_f values are lower compared to the 38.0 T typical of bulk goethite, and this is indeed related to the nanosized nature of the samples. Moreover, a further reduction in the H_f value was registered for the doped samples, suggesting a successful M-for-Fe substitution, as impurities are known to reduce the magnetic coupling between the Fe atoms in the crystals. Sample G[Zn5] 300 K spectrum appears different from

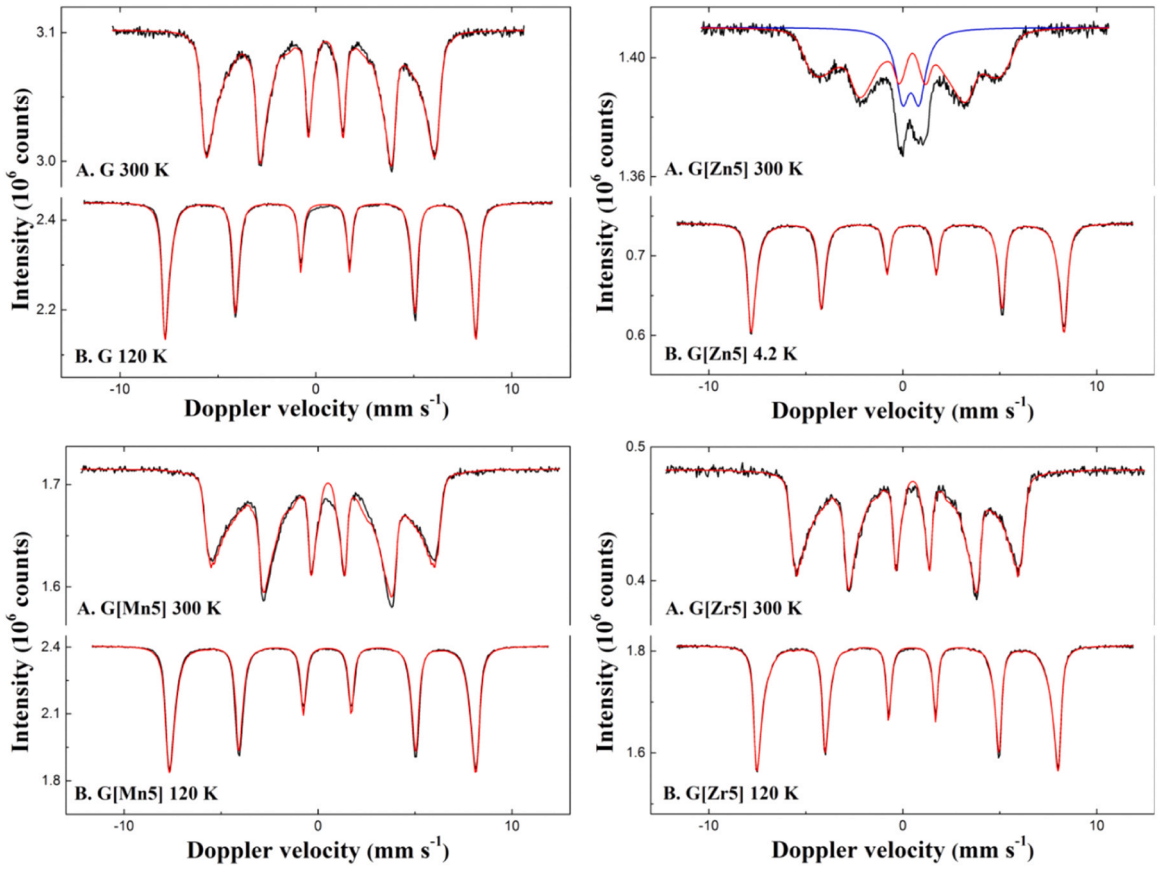

Fig. 4. MS spectra of the synthesized NPs measured at different temperatures (300, 120 and 4.2 K). Black lines represent the measured spectra, colored lines represent the fitted spectral contributions.

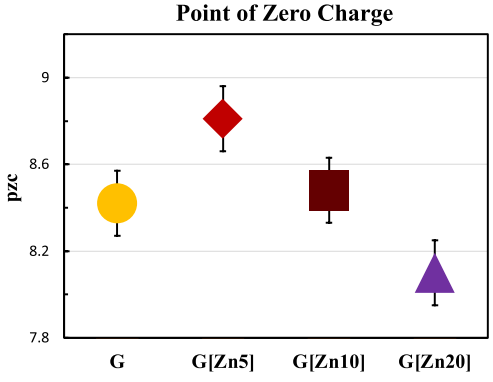

Fig. 5. pzc values estimated from the polynomial data interpolation.

the others, as its spectrum consists of a broad sextet ($\Gamma = 0.53$ mm s^{-1} compared to $\Gamma \sim 0.3$ mm s^{-1} of the other samples) and a doublet. This latter contribution represents a paramagnetic-like behavior, suggesting that either two different phases are coexisting, or the magnetic coupling was more reduced for Zn substitution compared to Mn and Zr. Thus, a measurement at 4.2 K was performed on G[Zn5], which proved the sample to consist of one unique phase of homogeneously Zn-doped goethite, as inferable from the unique sharp sextet and the retrieved fitting parameters. For the other samples, measurements at 120 K were enough to confirm that G consisted of pure goethite, while G[Mn5] and G[Zr5] consisted of unique Mn-doped and Zr-doped goethite phases, respectively. In particular, the reduction in the average H_f value of G[Mn5] compared to that of G suggests that Mn entered into the goethite structure as Mn^{3+}, as expected, based on previous studies [29,44, 60–63].

3.1.5. *Point of zero charge*

The pzc of the different samples estimated with both the polynomial (degree 4) and linear interpolations (see Figure S.2) are reported in Table S.1and Fig. 5.

Both approaches show agreement in the pzc determination, except for G[Zr5] with a deviation within the errors and thus does not affecting the overall trend, which is G[Zn5] > G > G[Mn5] > G[Zr5]. This is contrary to what was hypothesized, a higher oxidation state to favor a more positive surface charge (higher pzc) in goethite, since Zn, Mn and

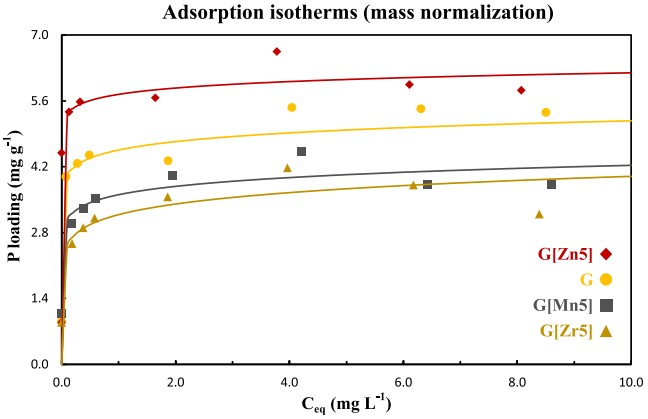

Fig. 6. Freundlich (solid line) and Langmuir (dashed line) adsorption isotherms with the duplicates data of the different synthesized NPs. Results are normalized with respect to the mass of adsorbent.

Table 4
MS reference values and fitting parameters of G, G[Zn5], G[Mn5] and G[Zr5] at 300 K, 120 K and 4.2 K.

Sample	T (K)	IS ($mm \cdot s^{-1}$)	QS ($mm \cdot s^{-1}$)	H_f (T)	Γ ($mm \cdot s^{-1}$)	Phase	Spectral contribution (%)
Bulk goethite reference values [59]	300	0.37	-0.26	38.0	-	-	-
	4.2	0.37	-0.25	50.6	-	-	-
G	300	0.38	-0.26	32.4*	0.28	α-FeOOH	100
	120	0.36	-0.24	48.9*	0.26	α-FeOOH	100
G[Zn5]	300	0.38	-0.24	24.6*	0.53	α-(Zn,Fe)OOH Fe^{3+}	77
		0.42	0.85^	-	0.85		23
	4.2	0.35	-0.21	49.6*	0.32	α-(Zn,Fe)OOH	100
G[Mn5]	300	0.38	-0.27	29.8*	0.25	α-(Mn,Fe)OOH	100
	120	0.36	-0.25	48.4	0.29	α-(Mn,Fe)OOH	100
G[Zr5]	300	0.38	-0.27	30.9	0.26	α-(Zr,Fe)OOH	100
	120	0.36	-0.24	46.9	0.23	α-(Zr,Fe)OOH	100

Experimental uncertainties: Isomer shift: I.S. ± 0.01 mm s^{-1}; Quadrupole splitting: Q.S. ± 0.01 mm s^{-1}; Line width: Γ ± 0.01 mm s^{-1}; Hyperfine fields: ± 0.1 T; Spectral contribution: ± 3 %. *Average magnetic field. ^Fixed value.

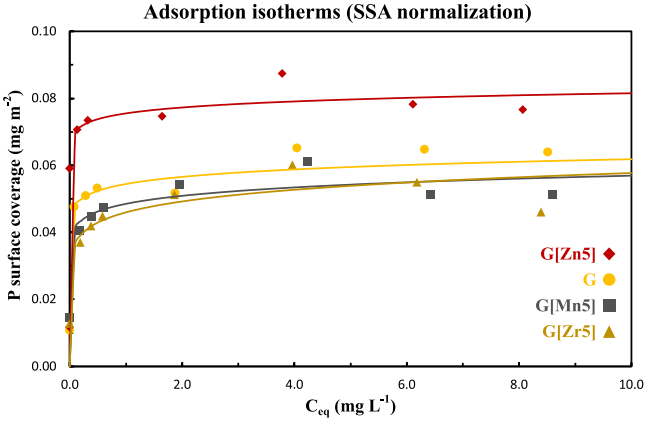

Fig. 7. Freundlich (solid line) and Langmuir (dashed line) adsorption isotherms with the duplicates data of the different synthesized NPs. Results are normalized with respect to the SSA of adsorbent.

Zr Pauling's electronegativity values are similar, (1.5–1.6 [64]), and lower than that of Fe (1.8). However, a similar result was obtained by Mohapatra et al. [31], which observed an increase in the pzc of goethite when doping with Cu^{2+}, while the opposite was observed when doping with Ni^{2+}. This effect could be explained by hypothesizing a higher surface protonation in G[Zn5], due to a charge compensation mechanism in Zn^{2+}-for-Fe^{3+} substitution, as proposed by Giovanoli et al. [29]. These results suggest G[Zn5] having a "more positive" surface charge in the pH range 6–8 of interest for freshwater bodies and WWTP effluents, while the opposite holds for G[Zr5], which would transition from weakly positive to weakly negative. This could be due to the opposite trend, in which Zr^{4+}-doped goethite might retain more OH^- surface groups, as a charge compensation mechanism or others, as a similar result was observed for Al^{3+}-doped goethite [65].

3.2. Adsorption experiments

Fig. 6 shows the adsorption isotherms per unit mass for all the NPs samples, with the fitted Langmuir and Freundlich curves, fitting parameter values are reported in Table 4. Both models seem to describe the adsorption trends well, probably due to the low adsorbent concentrations involved in the experiments (maximum SSA P coverages between 20 % and 30 %) and relative homogeneity of the different NPs surface morphologies. Nevertheless, it is important to remind that the two models face several limitations, and their application and fitting parameter values are meant just to help with the comparison and should be interpreted in relative rather than absolute terms. The adsorption trend is the same as that observed for the pzc: G[Zn5] > G > G[Mn5] > G[Zr5], as reflected by the fitting parameters: q_{max}, K_L, K_F and n^{-1}. Focusing on the affinity constant K_L, it is visible that goethite affinity for P has not been compromised by Zn-doping (actually slightly improved), while a reduction to a less than a third was observed with both Mn and Zr. This might be related to the higher pzc of G[Zn5], meaning that the more positive surface charge is able to attract more P.

Fig. 7 shows the adsorption isotherms per SSA, and the fitting parameters are reported in Table 5. Also in this case, G[Zn5] shows the highest P adsorbed, about 50 % higher (both per mass and SSA) compared to the others. This suggests G[Zn5] to have a more efficient surface for P adsorption, with the more positive charge able to attract more P, and possibly a higher site density or wider functional crystal faces for P adsorption. Further, this shows that SSA is not directly related to the adsorption performances, hence not being a determining factor for the adsorption capacity.

3.3. Regeneration experiments

The regeneration tests followed an adsorption experiment that consistently reproduced the trends observed in the isotherm experiments, both per mass and per SSA, as visible in Figure S.3 and Table S.2.

These results translate in a higher P surface coverage of about 33 % for G[Zn5], while a similar coverage between 22 % and 24 % were observed for the other samples, further corroborating the higher

Table 5
Langmuir and Freundlich fitting parameter of G, G[Zn5], G[Mn5] and G[Zr5] adsorption isotherms normalized to the mass of the adsorbent, with the relative RMSPE.

Sample	Langmuir			Freundlich		
	q_{max} [$mg\ g^{-1}$]	K_L [$L\ mg^{-1}$]	RMSPE	n	K_F [$(mg\ g^{-1})(mg\ L^{-1})^{-n}$]	RMSPE
G	5	47	0.34	0.06	5	0.34
G[Zn5]	6	49	0.47	0.03	6	0.47
G[Mn5]	4	15	0.34	0.07	4	0.34
G[Zr5]	4	10	0.34	0.10	3	0.34

Table 6
Langmuir and Freundlich fitting parameter of G, G[Zn5], G[Mn5] and G[Zr5] adsorption isotherms normalized to the SSA of the adsorbent, with the relative RMSPE.

Sample	Langmuir			Freundlich		
	q_{max} [mg m^{-2}]	K_L [L mg^{-1}]	RMSPE	n	K_F [(mg m^{-2})(mg L^{-1})$^{-n}$]	RMSPE
G	0.06	47	0.34	0.06	0.05	0.34
G[Zn5]	0.08	49	0.47	0.03	0.08	0.47
G[Mn5]	0.06	15	0.34	0.07	0.05	0.34
G[Zr5]	0.06	10	0.34	0.10	0.05	0.34

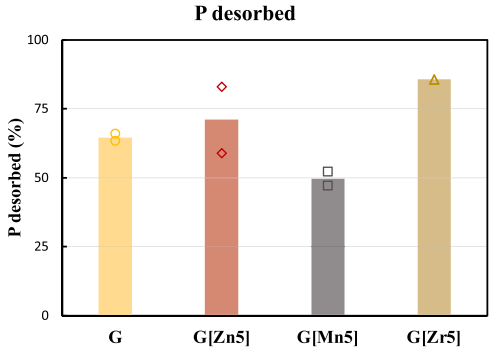

Fig. 8. Desorbed P and relative surface hindrance of undesorbed P of samples G, G[Zn5], G[Mn5] and G[Zr5].

Table 7
Desorbed P and relative surface hindrance of undesorbed P of samples G, G [Zn5], G[Mn5] and G[Zr5].

Sample	P desorbed % w/w	% SSA still covered
G	65 ± 1	6.8 ± 0.7
G[Zn5]	71 ± 12	8 ± 4
G[Mn5]	50 ± 4	10.7 ± 0.6
G[Zr5]	86 ± 8	2.2 ± 1

adsorption sites density of G[Zn5].

The regeneration tests, desorption percentages reported in Table 6 and Fig. 8, show the following trend: G[Zr5] > G[Zn5] ≳ G > G[Mn5]. This means that samples G[Zn5] and G[Zr5] did not require more effort for the regeneration compared to G, suggesting that no different P removal mechanism, such as precipitation, was promoted by the dopant. Sample G[Mn5], however, displayed the lowest desorption potential, and it is not to be excluded that a stronger bond or other mechanisms like surface precipitation might have happened. We conclude from these results that that Zn- and Zr- doping did not affect the P bonding mechanism to the extent of requiring more or less effort for desorption. Table 7.

3.4. Mössbauer spectroscopy on regenerated samples

The MS measurements of the regenerated samples were performed only at 300 K, as this was sufficient to draw conclusions, with the exception of sample G[Zn5], for similar reasons as explained in Section 3.4. The spectra are shown in Figure S.4 while the fitting parameters from data analysis are reported in Table S.3. G, G[Mn5], and G[Zr5] appeared to still consist of goethite-like phase, with slight differences ascribable to increased NPs size, probably due to sintering during centrifugation and oven drying of the samples. Conversely, G[Zn5] shows a slightly different spectrum compared to that of the virgin sample, with a significantly reduced intensity of the doublet contribution. Hence, a further measurement at 120 K was performed to exclude the possibility that the sample consists now of two different goethite-like phases, a pure one, and a Zn-doped one, or of another iron oxide phase. However, G[Zn5] displays a lower mean $H_f = 46.5$ T value compared to that of G, $H_f = 48.9$ T, at 120 K, and since no Fe and Zn dissolution was observed throughout the whole process, it was considered to have remained stable. Also in this case, NPs sintering might have taken place, as well as improved crystallinity, due to the observed reduction of Γ. From MS analysis it could be concluded that all the samples remain in the goethite-like phase, possibly preserving the level of doping, as no Zn, Mn or Zr was detected by the ICP in any solution. Further investigation at higher desorption pH values and multiple regeneration is needed, to obtain a rough estimation of the lifespan of the adsorbent.

Finally, further consistent comparative studies on goethite doping, both using different elements and doping percentages, are recommended to better understand the effect of the different dopant features on the overall goethite properties. Also, providing a support, such as ion exchange resins (i.e., the commercially available hybrid anion exchange adsorbents, HAIX), would allow to perform multiple adsorption/desorption tests, better estimating the reusability and life span of the adsorbent, while providing application to such nanoparticles in real-life systems.

4. Conclusions

The characteristics and adsorption properties of pure and doped goethite NPs using elements of different preferential oxidation states were investigated. A successful M-for-Fe substitution was obtained for all the elements, i.e., Zn^{2+}, Mn^{3+} and Zr^{4+}, although Zr displayed a lower substitution than targeted. This latter observation was ascribed to a combination of substitution mechanism and size and charge differences between Zr^{4+} and Fe^{3+}. It was observed that Zn^{2+}-doping increased the pzc of goethite, probably as a combination of protonation, as a charge compensation mechanism, and preferential growth of goethite crystal faces with high functional site density. This effect resulted in improved adsorption performances in terms of capacity, both per mass and per SSA, and affinity. It was also highlighted that SSA is not a determining factor for the adsorption capacity. Conversely, Mn^{3+} and Zr^{4+} doping caused a decrease in pzc and P-adsorption performance. The desorption test showed on average improved P-desorption for Zn^{2+}- and Zr^{4+}-doped goethite, while a decrease in desorption was observed for Mn^{3+}. This consistent comparative study shows the promising effects of Zn-doping for developing an effective and stable goethite-based adsorbent and provides insights on how to employ doping as a strategy to manipulate iron oxide surface properties.

CRediT authorship contribution statement

Carlo Belloni: Conceptualization, Methodology, Investigation, Validation, Data curation, Writing – original draft, Visualization. **Leon Korving:** Conceptualization, Methodology, Writing – review & editing, Supervision. **Geert-Jan Witkamp:** Conceptualization, Methodology, Writing – review & editing, Supervision. **Ekkes Brück:** Conceptualization, Methodology, Writing – review & editing, Supervision. **Iulian Dugulan:** Conceptualization, Methodology, Writing – review & editing, Supervision.

Declaration of Competing Interest

The authors declare the following financial interests/personal relationships which may be considered as potential competing interests: Carlo Belloni reports financial support was provided by Netherlands Organization for Scientific Research.

Data availability

Data will be made available on request.

Acknowledgements

This work was performed in the cooperation framework of Wetsus, European Centre of Excellence for Sustainable Water Technology (www.wetsus.nl). Wetsus is co-funded by the Dutch Ministry of Economic Affairs and Ministry of Infrastructure and Environment, the European Union Regional Development Fund, the Province of Fryslân and the Northern Netherlands Provinces. This research received funding from the Netherlands Organization for Scientific Research (NWO) in the framework of the Innovation Fund for Chemistry, and from the Ministry of Economic Affairs and Climate Policy in the framework of the TKI/PPS-Toeslagregeling. The authors thank the participants of the research theme "Phosphate recovery" for the interest, fruitful discussions, and financial support. A special thanks goes to Pim de Jager and Raimonda Buliauskaitė (Aquacare) for the frequent knowledge exchange and interest in the research, Harm van der Kooi for the technical support, Michel Steenvoorden and Maxim Ariens for the support with Mössbauer spectroscopy related matters, Kees Goubitz (TU Delft) for the support on XRD, Wiel Evers (TU Delft) for the TEM measurements, Jouk Jansen (TU Delft) for the support with SAED analysis, Renata van der Weijden (WUR) for the fruitful discussions, Prashanth Suresh Kumar (Plaksha University) and Terica Sinclair for the support and guidance, Amandine Dronne, Varad Kapur, Maddalena Tigli for the work done together.

Appendix A. Supporting information

Supplementary data associated with this article can be found in the online version at doi:10.1016/j.jece.2023.110505.

References

[1] D.W. Schindler, Evolution of phosphorus limitation in lakes, Science 195 (1977) 260–262, https://doi.org/10.1126/science.195.4275.260.
[2] L. Carvalho, C. Mcdonald, C. De Hoyos, U. Mischke, G. Phillips, G. Abor Borics, S. Poikane, B. Skjelbred, A.L. Solheim, J. Van Wichelen, A.C. Cardoso, Sustaining recreational quality of European lakes: minimizing the health risks from algal blooms through phosphorus control On secondment from CEH 2 to JRC 1, J. Appl. Ecol. 50 (2013) 315–323, https://doi.org/10.1111/1365-2664.12059.
[3] J.N. Pretty, C.F. Mason, D.B. Nedwell, R.E. Hine, S. Leaf, R. Dils, Environmental costs of freshwater eutrophication in England and Wales, Environ. Sci. Technol. 37 (2003) 201–208, https://doi.org/10.1021/es020793k.
[4] W.K. Dodds, W.W. Bouska, J.L. Eitzmann, T.J. Pilger, K.L. Pitts, A.J. Riley, J. T. Schloesser, D.J. Thornbrugh, Eutrophication of U. S. freshwaters: analysis of potential economic damages, Environ. Sci. Technol. 43 (2009) 12–19, https://doi.org/10.1021/es801217q.
[5] S.R. Carpenter, Phosphorus control is critical to mitigating eutrophication, Proc. Natl. Acad. Sci. USA 105 (2008) 11039–11040, https://doi.org/10.1073/pnas.0806112105.
[6] EC, Critical Raw Materials, 2020. https://doi.org/10.1007/978–3-030–40268-6_9.
[7] USGS, Mineral Commodity Summaries, 2020. https://pubs.usgs.gov/periodicals/mcs2020/mcs2020.pdf.
[8] D. Cordell, J.O. Drangert, S. White, The story of phosphorus: global food security and food for thought, Glob. Environ. Chang 19 (2009) 292–305, https://doi.org/10.1016/J.GLOENVCHA.2008.10.009.
[9] EC, European Green Deal, 2020. https://doi.org/10.4324/9780080495781–12.
[10] ECCircular Economy Action Plan, 2020. https://doi.org/10.7312/columbia/9780231167352.003.0015.
[11] EC, The Urban Waste Water Treatment Directive, 1992.
[12] P.S. Kumar, L. Korving, M.C.M. van Loosdrecht, G.J. Witkamp, Adsorption as a technology to achieve ultra-low concentrations of phosphate: research gaps and economic analysis, Water Res. X 4 (2019), 100029, https://doi.org/10.1016/J.WROA.2019.100029.
[13] R.M. Cornell, U. Schwertmann, Iron Oxides (2003), https://doi.org/10.1002/3527602097.
[14] P. Loganathan, S. Vigneswaran, J. Kandasamy, N.S. Bolan, Removal and recovery of phosphate from water using sorption, Crit. Rev. Environ. Sci. Technol. 44 (2014) 847–907, https://doi.org/10.1080/10643389.2012.741311.
[15] X. Wang, F. Liu, W. Tan, W. Li, X. Feng, D.L. Sparks, Characteristics of phosphate adsorption-desorption onto ferrihydrite: comparison with well-crystalline fe (Hydr) oxides, Soil Sci. 178 (2013) 1–11, https://doi.org/10.1097/SS.0b013e31828683f8.
[16] O.K. Borggaard, A.L. Gimsing, B.W. Strobel, Influence of humic substances on phosphate adsorption by aluminium and iron oxides 127 (2005) 270–279, https://doi.org/10.1016/j.geoderma.2004.12.011.
[17] P. Suresh Kumar, T. Prot, L. Korving, K.J. Keesman, I. Dugulan, M.C.M. van Loosdrecht, G.J. Witkamp, Effect of pore size distribution on iron oxide coated granular activated carbons for phosphate adsorption – Importance of mesopores, Chem. Eng. J. 326 (2017) 231–239, https://doi.org/10.1016/j.cej.2017.05.147.
[18] F.A. Ponce, D.P. Bour, Nitride-based semiconductors for blue and green light-emitting devices, Nature 386 (1997) 351–359, https://doi.org/10.1038/386351a0.
[19] K. Sivula, R. Van De Krol, Semiconducting materials for photoelectrochemical energy conversion, Nat. Rev. Mater. 1 (2016), https://doi.org/10.1038/natrevmats.2015.10.
[20] K. Zhang, J. Robinson, Doping of Two-Dimensional Semiconductors: A Rapid Review and Outlook, (2019). https://doi.org/10.1557/adv.2019.391.
[21] S. Rahim Pouran, A.A. Abdul Raman, W.M.A.Wan Daud, Review on the application of modified iron oxides as heterogeneous catalysts in Fenton reactions, J. Clean. Prod. 64 (2014) 24–35, https://doi.org/10.1016/j.jclepro.2013.09.013.
[22] L.F. Liotta, M. Gruttadauria, G. Di Carlo, G. Perrini, V. Librando, Heterogeneous catalytic degradation of phenolic substrates: catalysts activity, J. Hazard. Mater. 162 (2009) 588–606, https://doi.org/10.1016/j.jhazmat.2008.05.115.
[23] M. Zhu, I.E. Wachs, A perspective on chromium-Free iron oxide-based catalysts for high temperature water-gas shift reaction, Catal. Today 311 (2018) 2–7, https://doi.org/10.1016/j.cattod.2017.08.042.
[24] D.W. Lee, M.S. Lee, J.Y. Lee, S. Kim, H.J. Eom, D.J. Moon, K.Y. Lee, The review of Cr-free Fe-based catalysts for high-temperature water-gas shift reactions, Catal. Today 210 (2013) 2–9, https://doi.org/10.1016/j.cattod.2012.12.012.
[25] S. Krehula, M. Ristić, S. Kubuki, Y. Iida, L. Kratofil Krehula, S. Musić, The effects of In3+ doping on the properties of precipitated goethite, J. Alloy. Compd. 658 (2016) 41–48, https://doi.org/10.1016/j.jallcom.2015.10.191.
[26] E. Murad, J. Cashion, Mössbauer Spectroscopy of Environmental Materials and Their Industrial Utilization, Kluwer Academic Publishers, Dordrecht, 2004.
[27] E. Murad, L.H. Bowen, Magnetic ordering in Al-rich goethites: influence of crystallinity, Am. Miner. 72 (1987) 194–200.
[28] H. Liu, T. Chen, R.L. Frost, An overview of the role of goethite surfaces in the environment, Chemosphere 103 (2014) 1–11, https://doi.org/10.1016/J.CHEMOSPHERE.2013.11.065.
[29] R. Giovanoli, R.M. Cornell, Crystallization of metal substituted ferrihydrites, Z. Für Pflanzenernährung. Und Bodenkd. 155 (1992) 455–460, https://doi.org/10.1002/jpln.19921550517.
[30] A. Manceau, M.L. Schlegel, M. Musso, V.A. Sole, C. Gauthier, P.E. Petit, F. Trolard, Crystal chemistry of trace elements in natural and synthetic goethite, Geochim. Cosmochim. Acta 64 (2000) 3643–3661, https://doi.org/10.1016/S0016-7037(00)00427-0.
[31] M. Mohapatra, S.K. Sahoo, S. Anand, R.P. Das, Removal of As(V) by Cu(II)-, Ni(II)-, or Co(II)-doped goethite samples, J. Colloid Interface Sci. 298 (2006) 6–12, https://doi.org/10.1016/j.jcis.2005.11.052.
[32] M.A. Wells, R.W. Fitzpatrick, R.J. Gilkes, Thermal and mineral properties of A1-, Cr-, Mn-, Ni- and Ti-substituted goethite, Clays Clay Miner. 54 (2006) 176–194, https://doi.org/10.1346/CCMN.2006.0540204.
[33] P.G. Belelli, S.A. Fuente, N.J. Castellani, Phosphate adsorption on goethite and Al-rich goethite, Comput. Mater. Sci. 85 (2014) 59–66, https://doi.org/10.1016/j.commatsci.2013.12.030.
[34] E. Murad, U. Schwertmann, The influence of aluminium substitution and crystallinity on the Mössbauer spectra of goethite, Clay Miner. (1983) 301–312.
[35] S.A. Fysh, P.E. Clark, Aluminous goethite: a Mössbauer study, Phys. Chem. Miner. 8 (1982) 180–187, https://doi.org/10.1007/BF00308241.
[36] D.E. Latta, J.E. Bachman, M.M. Scherer, Fe electron transfer and atom exchange in goethite: influence of Al-substitution and anion sorption, Environ. Sci. Technol. 46 (2012) 10614–10623, https://doi.org/10.1021/es302094a.
[37] J. Xu, L.K. Koopal, M. Wang, J. Xiong, J. Hou, Y. Li, W. Tan, Phosphate speciation on Al-substituted goethite: ATR-FTIR/2D-COS and CD-MUSIC modeling, Environ. Sci. Nano. 6 (2019) 3625, https://doi.org/10.1039/c9en00539k.
[38] A.C. Scheinost, D.G. Schulze, I., U. Schwertmann, Diffuse Reflectance Spectra of Al Substituted Goethite: a Lingad Field Approach, 1999.
[39] L.-C. Hsu, Y.-M. Tzou, M.-S. Ho, C. Sivakumar, Y.-L. Cho, W.-H. Li, P.-N. Chiang, H. Y. Teah, Y.-T. Liu, Preferential phosphate sorption and Al substitution on goethite, Environ. Sci. Nano. 7 (2020) 3497, https://doi.org/10.1039/c9en01435g.
[40] D.C. Golden, L.H. Bowen, S.B. Weed, J.M. Bigham, Mössbauer studies of synthetic and soil-occurring aluminum-substituted goethites, Soil Sci. Soc. Am. J. 43 (1979) 802–808, https://doi.org/10.2136/sssaj1979.03615995004300040038x.
[41] C.C. Ainsworth, M.E. Sumner, Effect of aluminum substitution in goethite on phosphorus adsorption: II. Rate of adsorption, Soil Sci. Soc. Am. J. 49 (1985) 1149–1153, https://doi.org/10.2136/sssaj1985.03615995004900050015x.
[42] H.D. Ruan, R.J. Gilkes, Kinteics of Thermal Dehydroxylation of Aluminous Goethite, 1996.

[43] M. Ma, H. Gao, Y. Sun, M. Huang, The adsorption and desorption of Ni(II) on Al substituted goethite, J. Mol. Liq. 201 (2015) 30–35, https://doi.org/10.1016/J.MOLLIQ.2014.11.024.
[44] W. Stiers, U. Schwertmann, Evidence for manganese substitution in synthetic goethite, Geochim. Cosmochim. Acta 49 (1985) 1909–1911, https://doi.org/10.1016/0016-7037(85)90085-7.
[45] K. Rout, A. Dash, M. Mohapatra, S. Anand, Manganese doped goethite: structural, optical and adsorption properties, J. Environ. Chem. Eng. 2 (2014) 434–443, https://doi.org/10.1016/j.jece.2014.01.001.
[46] X. Zhang, L. Zhang, Y. Liu, M. Li, X. Wu, T. Jiang, C. Chen, Y. Peng, Mn-substituted goethite for uranium immobilization: a study of adsorption behavior and mechanisms, Environ. Pollut. 262 (2020), https://doi.org/10.1016/j.envpol.2020.114184.
[47] X. Sun, H.E. Doner, M. Zavarin, Spectroscopy Study of Arsenite [As(III)] Oxidation on Mn-substituted Goethite, 1999.
[48] R.E. Vandenberghe, A.E. Verbeeck, E. De Grave, W. Stiers, 57Fe Mössbauer effect study of Mn-substituted goethite and hematite, Hyperfine Inter. 29 (1986) 1157–1160, https://doi.org/10.1007/BF02399440.
[49] S. Krehula, S. Musić, Ž. Skoko, S. Popović, The influence of Zn-dopant on the precipitation of α-FeOOH in highly alkaline media, J. Alloy. Compd. 420 (2006) 260–268, https://doi.org/10.1016/J.JALLCOM.2005.10.019.
[50] M. Villacis-Garcia, M. Ugalde-Arzate, K. Vaca-Escobar, M. Villalobos, R. Zanella, N. Martinez-Villegas, Laboratory synthesis of geothite ad ferrihydrite of controlled partocel sozes, Bol. La Soc. Geol. Mex. 67 (2015) 433–446.
[51] Z. Klencsár, Mössbauer spectrum analysis by evolution algorithm, Nucl. Instrum. Methods Phys. Res. Sect. B Beam Interact. Mater. At. 129 (1997) 527–533, https://doi.org/10.1016/S0168-583X(97)00314-5.
[52] T. Mahmood, M.T. Saddique, A. Naeem, P. Westerhoff, S. Mustafa, A. Alum, Comparison of different methods for the point of zero charge determination of NiO, Ind. Eng. Chem. Res. 50 (2011) 10017–10023, https://doi.org/10.1021/ie200271d.
[53] W.F. Tan, S.J. Lu, F. Liu, X.H. Feng, J.Z. He, L.K. Koopal, Determination of the point-of-zero charge of manganese oxides with different methods including an improved salt titration method, Soil Sci. 173 (2008) 277–286, https://doi.org/10.1097/SS.0b013e31816d1f12.
[54] I. Langmuir, The adsorption of gases on plane surfaces of glass, mica and platinum, Res. Lab. Gen. Electr. Co. (1918). ⟨https://pubs.acs.org/sharingguidelines⟩.
[55] H. Freundlich, Über die Adsorption in Lösungen, Zeitschrift Für Phys. Chemie. (1907).
[56] D.S. Tawfik, R.E. Viola, Arsenate replacing phosphate: alternative life chemistries and ion promiscuity, Biochemistry 50 (2011) 48, https://doi.org/10.1021/bi200002a.
[57] R.D. Shannon, Revised effective ionic radii and systematic studies of interatomic distances in halides and chalcogenides, Acta Cryst. (1976), https://doi.org/10.1107/S0567739476001551.
[58] N. Popov, M. Ristić, M. Robić, V. Gilja, L. Kratofil Krehula, S. Musić, S. Krehula, Synthesis and properties of Sn-doped α-FeOOH nanoparticles, Chem. Pap. 75 (2021) 6355–6366, https://doi.org/10.1007/s11696-021-01802-9.
[59] E. Murad, Magnetic properties of microcrystalline iron (III) oxides and related materials as reflected in their Mössbauer spectra, Phys. Chem. Miner. 23 (1996) 248–262, https://doi.org/10.1007/bf00207766.
[60] A.C. Scheinost, H. Stanjek, D.G. Schulze, U. Gasser, D.L. Sparks, Structural environment and oxidation state of Mn in goethic-groutite solid-solutions, Am. Miner. 86 (2001) 139–146, https://doi.org/10.2138/am-2001-0115.
[61] U.G. Gasser, R. Nüesch, M.J. Singer, E. Jeanroy, Distribution of manganese in development, Clay Miner. 34 (1999) 291–299.
[62] R.M. Cornell, R. Giovanoli, Effect of manganese on the transformation of ferrihydrite into goethite and jacobsite in alkaline media, Clays Clay Miner. 35 (1987) 11–20, https://doi.org/10.1346/CCMN.1987.0350102.
[63] J. Gerth, Unit-cell dimensions of pure and trace metal-associated goethites, Geochim. Cosmochim. Acta 54 (1990) 363–371, https://doi.org/10.1016/0016-7037(90)90325-F.
[64] W. Gosdy, W.J.Orville Thomas, Electronegativities of the elements, J. Chem. Phys. 24 (1956) 439–444, https://doi.org/10.1063/1.1742493.
[65] W. Li, L. Wang, F. Liu, X. Liang, X. Feng, W. Tan, L. Zheng, H. Yin, Effects of Al3 + doping on the structure and properties of goethite and its adsorption behavior towards phosphate, J. Environ. Sci. 45 (2015) 18–27, https://doi.org/10.1016/j.jes.2015.12.013.